

University of Texas Rio Grande Valley

**ScholarWorks @ UTRGV**

---

Mechanical Engineering Faculty Publications  
and Presentations

College of Engineering and Computer Science

---

1-15-2010

## **Recovery of rectified signals from hot-wire/film anemometers due to flow reversal in oscillating flows**

Yingchen Yang

Douglas L. Jones

Chang Liu

Follow this and additional works at: [https://scholarworks.utrgv.edu/me\\_fac](https://scholarworks.utrgv.edu/me_fac)



Part of the [Mechanical Engineering Commons](#)

---

# Recovery of rectified signals from hot-wire/ film anemometers due to flow reversal in oscillating flows

Cite as: Rev. Sci. Instrum. **81**, 015104 (2010); <https://doi.org/10.1063/1.3277109>

Submitted: 11 June 2009 • Accepted: 03 December 2009 • Published Online: 15 January 2010

Yingchen Yang, Douglas L. Jones and Chang Liu



View Online

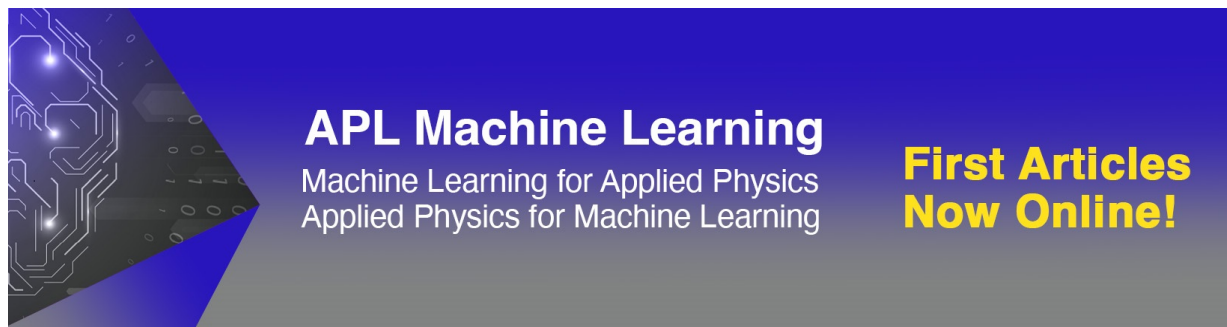


Export Citation

## ARTICLES YOU MAY BE INTERESTED IN

[A hot-film air flow sensor for elevated temperatures](#)

Review of Scientific Instruments **90**, 015007 (2019); <https://doi.org/10.1063/1.5065420>



**APL Machine Learning**  
Machine Learning for Applied Physics  
Applied Physics for Machine Learning

**First Articles  
Now Online!**

## Recovery of rectified signals from hot-wire/film anemometers due to flow reversal in oscillating flows

Yingchen Yang,<sup>1,a)</sup> Douglas L. Jones,<sup>2</sup> and Chang Liu<sup>1,b)</sup>

<sup>1</sup>Department of Mechanical Engineering, Northwestern University, Evanston, Illinois 60208, USA

<sup>2</sup>Department of Electrical and Computer Engineering, University of Illinois at Urbana-Champaign, Urbana, Illinois 61801, USA

(Received 11 June 2009; accepted 3 December 2009; published online 15 January 2010)

Hot-wire/film anemometers have been broadly used in experimental studies in fluid mechanics, acoustics, and ocean engineering. Yet, it is well known that hot-wire/film anemometers rectify the signal outputs due to the lack of sensitivity to flow direction. This main drawback, in turn, makes them less useful for diverse fluctuating flow measurements. To solve this issue, a rectification recovery method has been developed based on reconstruction of the Fourier series expansion in conjunction with signal-squaring approach. This signal recovery method was experimentally examined and proven to be successful for both conventional and microfabricated hot-wire/film anemometers. The method was further applied to dipole field measurements, with data from recovered signals perfectly matching the analytical model of the dipole field. © 2010 American Institute of Physics. [doi:10.1063/1.3277109]

### I. INTRODUCTION

Hot-wire/film anemometers (simply referred to as HWAs thereafter) have been used in fluid mechanics and acoustics studies for nearly a century. Conventional HWAs are widely available. In recent years, several micro-electro-mechanical system (MEMS)-based HWAs have been developed<sup>1-5</sup> and have been applied in fluid field measurements.<sup>6,7</sup>

However, HWAs suffer from a well-known inherent defect. Namely, they are unable to discern flow direction in a plane normal to the sensing filament—the hot wire. The cause lies in the fact that the heat loss from the hot wire by forced convection, therefore the HWA output, depends on the magnitude, not on the direction, of the local flow velocity. As a consequence, the signal output of a HWA is always rectified whenever a local oscillating flow changes direction. That accounts for the interference of the hot-wire-generated natural convection in the vertical direction. Coombs *et al.*<sup>8</sup> employed HWA to measure fish lateral line stimuli, a vibrating sphere generated dipole field, and reported the rectification issue. Muller<sup>9</sup> observed signal rectification while employing HWA for measurements of a complex turbulent boundary layer. Yao *et al.*<sup>10</sup> compared HWA and laser Doppler anemometer measurements on synthetic jet flow and identified the rectification effect on HWA measurements.

Due to the broad application of HWAs and the widely encountered rectification issue, efforts have been made over years to make the HWAs direction-sensitive, as reviewed by Bruun.<sup>11</sup> One approach is to use double or triple wires to discern velocity. This approach is mostly restricted to bidirectional flow measurements. Pulsed-wire anemometers

(PWAs) have been developed following this idea.<sup>12</sup> Another approach is flying hot-wire anemometers (FHAs). In this approach, the hot-wire probe is moved along a trajectory so that a known velocity will be superimposed to stop local velocity reversal with respect to a FHA. Using this technique, Watmuff *et al.*<sup>13</sup> studied flow separation and recirculation zones behind bluff bodies. Recently, oscillating hot-wire anemometers (OHWs) have been developed to further enhance the discerning capability to flow directions.<sup>14,15</sup>

Yet, these approaches have their own disadvantages. For PWAs, the primary disadvantage is the limited bandwidth, which is at most around 100Hz. For FHAs and OHWs, due to the high-speed trajectory motion or oscillation, the hot wire may vibrate, and the probe interferes with the measured flow field. Besides, in many circumstances such motion arrangements are not feasible or practical.

Differing from the previous approaches of making hardware improvements, the present research aims at resolving the rectification issue by means of mathematical algorithm and software development. The main focus of our efforts is to develop a recovery/derectionification postprocessing method that can be used for both conventional and microfabricated HWAs for diverse flow measurements.

The developed derectionification method is expected to recover signals with distinct frequency components in the frequency domain, especially for low Reynolds number flows. In this paper the derectionification method is discussed based on measurements of a dipolar flow. Dipolar flows have been widely employed for fish behavioral studies.<sup>8,16</sup> The application of this derectionification method is not limited to dipolar flows. One big application area could be biofluid studies on swimming and flying animals. Such flow phenomena fall in the low Reynolds number regime. The beating fins<sup>17,18</sup> or flapping wings<sup>19,20</sup> of those animals generate well-organized vortical flow structures that present highly distinct dominant

<sup>a)</sup>Current address: Department of Engineering, University of Texas at Brownsville, Brownsville, TX 78520, USA.

<sup>b)</sup>Author to whom correspondence should be addressed. Electronic mail: changliu@northwestern.edu.

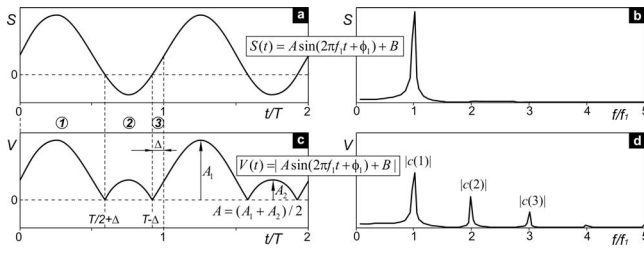


FIG. 1. Waveforms and corresponding amplitude spectra for a simulated sinusoidal signal before [(a) and (b)] and after [(c) and (d)] rectification.

frequencies with relatively low turbulent background noise. As a natural extension, HWAs and the signal recovery method can be applied to biomimetic studies on autonomous underwater vehicles<sup>21,22</sup> and microair vehicles, which are inspired by those swimming and flying animals. The recovery method is also applicable to some traditional research areas, such as in wave-structure interactions,<sup>23</sup> where the flows possess similar spectral patterns.

## II. DERECTIFICATION SCHEMES FOR IDEALIZED SIGNALS

Understanding rectification issue for idealized signals is important for developing fundamental derectification schemes. Such schemes, in turn, motivate the development of a comprehensive derectification method that can be used to recover real-world HWA signals.

### A. The signal rectification issue

Assume an ideal oscillating flow with no dc current, wherein particles of the fluid perform sinusoidal oscillation in a direction parallel to gravity. When a HWA is exposed in the flow with the sensing filament horizontally oriented, the flow velocity at the location of the hot wire consists of two components. Specifically, one is an ac component from the oscillating flow at the frequency of  $f_1$ ; another is a dc component due to natural convection generated by the hot wire itself. The total velocity  $S(t)$  can be expressed as

$$S(t) = A \sin(2\pi f_1 t + \phi_1) + B, \quad (1)$$

where  $t$  is the time,  $A$  is the amplitude of oscillating velocity ( $A > 0$ ),  $\phi_1$  is the initial phase angle, and  $B$  is the dc component of the velocity. The waveform and spectral distribution of the velocity are presented in Figs. 1(a) and 1(b), respectively. Correspondingly, the HWA senses this resultant velocity but rectifies it in the output. Note that the response of a HWA to local flow velocity is nonlinear.<sup>11</sup> Assume that the HWA faithfully recorded the local velocity fluctuation but with rectification. Then after the correction of HWA voltage output via calibration, the measured velocity  $V(t)$  can be expressed as

$$V(t) = |S(t)| = |A \sin(2\pi f_1 t + \phi_1) + B|. \quad (2)$$

Obviously, when  $A \leq |B|$ , the ac velocity component can be faithfully recorded by the HWA since there is no flow reversal. However, when  $A > |B|$ , rectification distorts the waveform [Fig. 1(c)] and introduces higher frequency components at multiples of  $f_1$  [Fig. 1(d)].

Note that in the above discussion the dc component  $B$  in Eq. (2) is due to a local flow caused by natural convection. In the case a mean flow is superimposed to the oscillating flow, it will have the same effect on the HWA signals.

### B. Derectification schemes for ideal signal input

At first glance, signal derectification appears to be straightforward. It is indeed the case with idealized signal input. We describe three preliminary schemes we have developed: one in the time domain and two in the frequency domain.

#### 1. Scheme 1: Derectification in time domain

In an idealized case as shown in Fig. 1(c), the rectified waveform can be recovered by taking the mirror image of every other hump with respect to  $V(t)=0$ . The amplitude of the recovered signal can be obtained by taking the summation of the magnitude of two adjacent peaks [ $A_1$  and  $A_2$  as marked in Fig. 1(c)] and multiplying by half.

#### 2. Scheme 2: Derectification in frequency domain by solving nonlinear equations

The second method uses Fourier series to establish nonlinear equations that interrelate signal features. The procedure is outlined below. First, Eq. (2) can be expressed in a Fourier series as

$$V(t) = \sum_{k=0}^{\infty} c(k) e^{j2\pi k(t/T)}, \quad (3)$$

where  $T$  is the period and  $T=1/f_1$ . The coefficients of the Fourier series are

$$c(k) = \frac{1}{T} \int_0^T V(t) e^{-j2\pi k(t/T)} dt. \quad (4)$$

The zero crossings of  $V(t)$  occur at  $t=T/2+\Delta$  and  $t=T-\Delta$ , which divide one period of waveform into three segments, as illustrated in Fig. 1(c). Solving for the coefficients of the Fourier series gives, for the first four terms,

$$c(0) = \frac{1}{T} \left[ \underbrace{\int_0^{T/2+\Delta} V(t) e^{-j2\pi k(t/T)} dt}_1 - \underbrace{\int_{T/2+\Delta}^{T-\Delta} V(t) e^{-j2\pi k(t/T)} dt}_2 + \underbrace{\int_{T-\Delta}^T V(t) e^{-j2\pi k(t/T)} dt}_3 \right] \\ = \frac{2}{\pi} \left( B \sin^{-1} \left( \frac{B}{A} \right) + A \sqrt{1 - \frac{B^2}{A^2}} \right), \quad (5)$$

$$c(1) = \frac{-j}{\pi} \left[ A \sin^{-1} \left( \frac{B}{A} \right) + B \sqrt{1 - \frac{B^2}{A^2}} \right], \quad (6)$$

$$c(2) = -2 \frac{(A^2 - B^2)}{3A\pi} \sqrt{1 - \frac{B^2}{A^2}}, \quad (7)$$

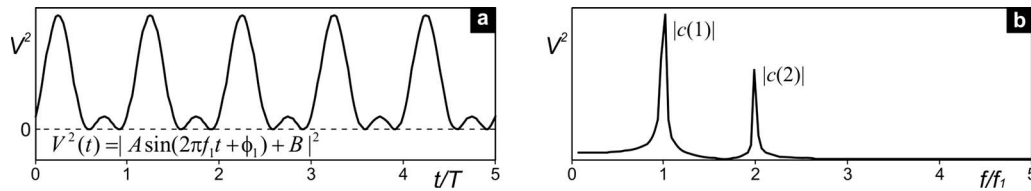


FIG. 2. Waveforms (left) and amplitude spectrum (right) of a simulated signal as defined in the waveform.  $B=0.5A$ ,  $f_1=50$  Hz, and  $\phi_1=0$ .

$$c(3) = -2jB \frac{(A^2 - B^2)}{3A^2\pi} \sqrt{1 - \frac{B^2}{A^2}}. \quad (8)$$

In Eqs. (5)–(8), the two unknowns  $A$  and  $B$  are defined in Eq. (2). For an experimentally acquired signal with rectification and with calibration, namely,  $V(t)$ , the coefficients  $c(1)$  through  $c(3)$  can be extracted by taking the fast Fourier transform (FFT) of the actual signal. Figure 1(d) shows the amplitude spectrum that includes the absolute values of the above coefficients at corresponding frequencies. In general cases, the first and second peaks  $|c(1)|$  and  $|c(2)|$  are dominant over others. Therefore, solving Eqs. (6) and (7) yields two unknowns  $A$  and  $B$ , leading to recovery of the rectified signal.

### 3. Scheme 3: Deredictification in frequency domain by squaring time trace of a signal

Another frequency-domain dervedictification approach involves squaring a HWA signal. This original approach of ours significantly benefits the development of an effective dervedictification method for complex real-world signals, which will be discussed in a later section.

For a rectified signal as defined in Eq. (2), taking square and expanding it give

$$V^2(t) = \underbrace{\frac{A^2}{2}}_{c(0)} + \underbrace{2AB \sin(2\pi f_1 t + \phi_1)}_{c(1)} + \underbrace{\frac{A^2}{2} \sin\left(4\pi f_1 t + 2\phi_1 - \frac{\pi}{2}\right)}_{c(2)}. \quad (9)$$

The waveform and amplitude spectrum [containing the absolute values of  $c(1)$  and  $c(2)$  at corresponding frequencies] of the squared signal are graphically presented in Figs. 2(a) and 2(b), respectively. With known  $c(1)$  and  $c(2)$ , which can be obtained from the FFT of the squared signal, one can derive both  $A$  and  $B$  by using the following equations:

$$A = \sqrt{2c(2)}, \quad (10)$$

$$B = \frac{c(1)}{2\sqrt{2c(2)}}. \quad (11)$$

### III. CHALLENGES OF REAL-WORLD SIGNALS

Although mathematically straightforward, the three schemes discussed in the foregoing are difficult to apply to real-world HWA signals. There are three major issues a successful algorithm needs to deal with: (i) rectification-induced high frequency components may not be faithfully recorded,

(ii) background noise may distort the signal severely, and (iii) circuits may introduce dc shift that will be superimposed to the rectified signals. These three issues are discussed further below.

The first issue is from experimental observation. HWAs, both conventional and MEMS-based, do not record rectification-caused frequency components over two times of stimulus frequency faithfully. In fact, a large amount of experimental results, as will be discussed in a later section, shows that in the frequency domain, the third peak and following ones have magnitudes much lower than expected. Experiments with different sampling rates on quite a wide range have been explored, but no noticeable improvement was found. Furthermore, by numerically simulating a rectified signal at the same sampling rate as used in experiments, all peaks in the frequency domain appeared as they were supposed to be. Obviously, it is not a sampling-rate problem. Also note that frequency responses of both conventional and MEMS-based HWAs used in our experiments are over 1000 Hz.<sup>4</sup> In contrast, we conducted measurements in oscillating flows with dominant frequencies below 100 Hz.

Although the reason is not clear yet, the loss of the higher-order peaks from HWA measurements can significantly change the waveform of a rectified signal. As illustrated in Figs. 3(a) and 3(b), a comparison is made between two simulated signals—a rectified sinusoidal signal with stimulus frequency  $f_1$  and the same signal with low-pass filtering at  $2.5f_1$ . Due to the elimination of peaks after the second one [Fig. 3(b)], the waveform of the filtered signal biases away from its original remarkably [Fig. 3(a)]. No doubt applying any of the three aforementioned schemes to the filtered signal will cause a large error.

The second issue is associated with background noise. In practice, the signal contents from HWA measurements on oscillating flows with dominant frequency  $f_1$  can be itemized as

$$V(t) = |A \sin(2\pi f_1 t + \phi_1) + B + \text{noise } 1| + C + \text{noise } 2, \quad (12)$$

where  $A \sin(2\pi f_1 t + \phi_1)$  is from the stimulus,  $B$  is caused by dc flow, noise 1 is mechanical noise,  $C$  is a circuit-introduced dc shift, and noise 2 is electrical noise.

The background noise distorts the waveform of a rectified signal. Therefore applying Scheme 1 to such signals becomes meaningless. For Scheme 3, signal squaring may cause severe interference between frequency components of interest and background noise. The yielded results might be useless.

The third issue to be discussed herein is the dc component introduced by the control circuit of a HWA. This dc

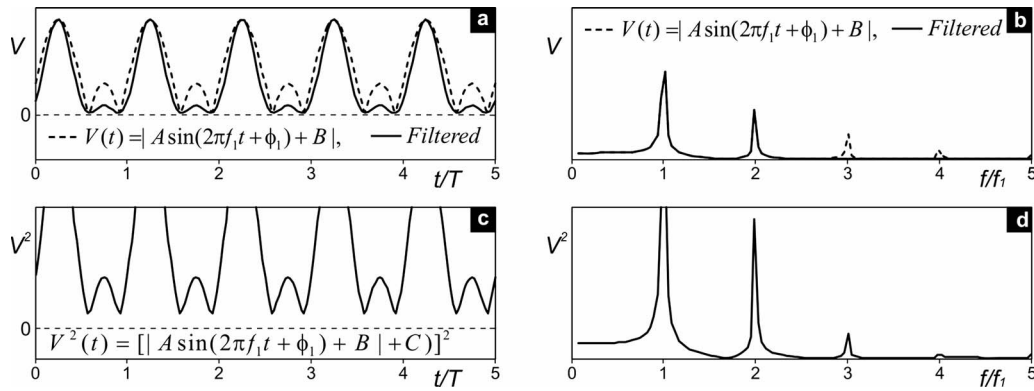


FIG. 3. Waveforms (left column) and corresponding amplitude spectra (right column) of a series of simulated signals as defined in each waveform. For all the plots,  $B=0.5A$ ,  $C=0.5A$ ,  $f_1=50$  Hz,  $\phi_1=0$ , and  $\phi_2=p/4$ .

component is added to the already rectified signal acquired from a HWA [Fig. 3(c)]. Recall that the rectified signal has a dc component itself. This makes it really difficult to properly remove the circuit-introduced dc. It is especially true when the waveform is distorted by the background noise. This additional dc alone does not affect Schemes 1 and 2 from functioning but disrupts Scheme 3 significantly. Specifically, it can dramatically change the magnitudes of peaks in frequency domain after signal squaring. This is evident by comparing Figs. 2(b) and 3(d), which are plotted in the same scale.

Note that in the foregoing discussion, physically existing higher harmonics has been ignored. In fact, higher harmonics, in contrast to the fundamental, broadly exist in various fluctuating flows; among them the second harmonic is the strongest. In general, the second harmonic overlaps with the rectification-caused frequency component at the same frequency but with different phase angles. It is possible to differentiate them by knowing or measuring their phase difference. However, this cannot be done using HWAs only. Fortunately, in most of fluctuating flows the second harmonics are at least an order lower in magnitude than their fundamentals.<sup>24</sup> Therefore, for the present approach, the effect of the second harmonic was not accounted for.

#### IV. RECTIFICATION SCHEME FOR REAL-WORLD SIGNALS

To overcome the limitations encountered in preliminary schemes, an advanced signal recovery method is developed. The core of this method is to preclude all nonrectification related frequency contents, e.g., background noise, and to reconstruct all rectification-induced frequency content. For reconstruction, the initial phase angles are obtained by applying analytically derived phase relationships, and corresponding amplitudes are determined by using Scheme 3—the signal-squaring scheme.

##### A. Phase-angle determination among rectification-induced frequency components

For a rectified periodic signal as defined in Eq. (2), the Fourier series expansion is of the form

$$\begin{aligned}
 V(t) = & A_0 + A_1 \sin(2\pi f_1 t + \phi_1) + A_2 \sin(4\pi f_1 t + \phi_2) \\
 & + A_3 \sin(6\pi f_1 t + \phi_3) + A_4 \sin(8\pi f_1 t + \phi_4) \\
 & + A_5 \sin(10\pi f_1 t + \phi_5) + \dots, \quad (13)
 \end{aligned}$$

where  $A_0, A_1, A_2, A_3, A_4,$  and  $A_5$  are some constants depending on  $A, B,$  and  $\phi_1$ . Note that  $A, B,$  and  $\phi_1$  are unknowns to be determined by recovery. Analytically  $\phi_2, \phi_3, \phi_4,$  and  $\phi_5$  can be derived as follows:

$$\phi_2 = 2\phi_1 - \pi/2, \quad (14)$$

$$\phi_3 = 3\phi_1, \quad (15)$$

$$\phi_4 = \begin{cases} 4\phi_1 - \pi/2, & (B/A < 0.41) \\ 4\phi_1 + \pi/2, & (B/A > 0.41), \end{cases} \quad (16)$$

$$\phi_5 = \begin{cases} 5\phi_1, & (B/A < 0.61) \\ 5\phi_1 + \pi, & (B/A > 0.61). \end{cases} \quad (17)$$

These equations show that  $\phi_2$  and  $\phi_3$  are functions of  $\phi_1$  only.  $\phi_4$  and  $\phi_5$  also solely depend on  $\phi_1$ , except that at some threshold points, the ratio of  $B$  over  $A$  functions as a switch. Additionally, at  $B/A=0.41$  the  $4f_1$  component disappears, and at  $B/A=0.61$  the  $5f_1$  component vanishes.

The independent nature of  $\phi_2$  through  $\phi_5$  from  $A$  and  $B$  is very useful on recovering a rectified signal. By extracting either  $\phi_1$  or  $\phi_2$  from the original signal, depending on which frequency component is more dominant or more reliable, initial phase information for all other rectification-caused frequency components can be derived using Eqs. (14)–(17). This makes it possible to reconstruct all the rectification-related frequency components. Such reconstruction process is critical to ensure an accurate recovery of a rectified signal, accounting for a number of issues discussed in the foregoing. Especially, for higher frequency components after  $2f_1$ , the amplitude attenuation needs to be compensated.

##### B. Amplitude determination among rectification-induced frequency components

By reconstruction, all the amplitudes in Eq. (13) need to be defined. The process starts with either  $f_1$  or  $2f_1$  component, whichever dominates. The amplitude and initial phase angle of this first treated frequency component can be de-

rived by means of an FFT of the real measured signal. Then the initial phase angle of the other frequency component can be obtained using Eq. (14). Its amplitude, on the other hand, needs to be determined based on a new criterion. That is, by subtracting this reconstructed frequency component from the original signal and taking the FFT, the magnitude of the peak at this specific frequency should be minimized.

Upon determination of  $A_1$  and  $A_2$  for reconstruction, the signal-squaring scheme is then employed as the only criterion for determining values for  $A_3$ ,  $A_4$ ,  $A_5$ , etc. This scheme has been discussed in Sec. II as a recovery method of an idealized rectified signal. However, here it is used for a different purpose. As shown in Fig. 1(d), an idealized rectified signal has an infinite number of peaks in the frequency domain. After squaring, however, only two peaks remain in addition to a dc component; all higher frequency components vanish. This unique feature has been presented analytically in Eq. (9) and graphically in Fig. 2(b). Using this feature as a criterion, one can tell if a reconstructed HWA signal in a step-by-step process is approaching an idealized rectified signal, as defined in Eq. (2).

More specifically, following reconstruction of  $A_3$ ,  $A_4$ ,  $A_5$ , etc.,  $A_i$  ( $i > 2$ ) should have a particular value. With this particular value, the reconstructed signal in the form of Eq. (13), but without terms after  $A_i$ , best represents an idealized rectified signal. In other words, squaring this partially reconstructed signal and taking the FFT should yield minimum sum of peak magnitudes after  $2f_1$ . In present discussion, reconstruction of frequency components up to  $5f_1$  is provided. The method can be extended to reconstruct more frequency components for better accuracy.

### C. Detailed approach

For reconstruction, the bottom line is to make sure that all frequency components comply with the phase relationships established in Eqs. (14)–(17), while maintaining maximum fidelity of the first ( $f_1$ ) and second ( $2f_1$ ) frequency components to the original signal. The detailed recovery process is summarized in the following. Symbols and expressions used are as defined in Eq. (13).

- (a) Acquire a signal and convert it from voltage to velocity by applying nonlinear calibration formulas (with more details in Sect. V A). The converted signal is defined as  $U(t)$ .
- (b) Extract amplitude and initial phase information of the two frequency components at  $f_1$  and  $2f_1$  by spectral analysis.
- (c) Re-extract the  $2f_1$  component based on information of  $f_1$  component from step (b).
  - (i) Designate the amplitude and initial phase angle of the  $f_1$  component as  $A_1$  and  $\phi_1$ .
  - (ii) Determine  $\phi_2$  from Eq. (14).
  - (iii) Determine  $A_2$  by making  $U(t) - A_2 \sin(4\pi f_1 t + \phi_2)$  have a minimal  $2f_1$  component.
  - (iv) Determine the amplitude of this minimal  $2f_1$  component.

- (d) Re-extract the  $f_1$  component based on information of the  $2f_1$  component from step (b).
  - (i) Designate the amplitude and initial phase angle of the  $2f_1$  component as  $A_2$  and  $\phi_2$ .
  - (ii) Determine  $\phi_1$  from Eq. (14).
  - (iii) Determine  $A_1$  by making  $U(t) - A_1 \sin(2\pi f_1 t + \phi_1)$  have a minimal  $f_1$  component.
  - (iv) Determine the amplitude of this minimal  $f_1$  component.
- (e) Take the values of  $(A_1, \phi_1)$  and  $(A_2, \phi_2)$  from step (c) or step (d), whichever gives a lower value in its substep (iv).
- (f) Calculate initial phase angles of all other frequency components at  $3f_1$ ,  $4f_1$ , and  $5f_1$  using Eqs. (15)–(17) and the value of  $\phi_1$  from step (e).
- (g) Determine the amplitude  $A_3$  of the  $3f_1$  component.
  - (i) Assign an initial value to  $A_3$ , noting that  $\phi_3$  becomes known from Eq. (15).
  - (ii) Reconstruct the signal by taking  $V(t) = \sum_{i=1}^3 A_i \sin(2i\pi f_1 t + \phi_i)$ .
  - (iii) Reset the zero level by subtracting the minimum value from the newly reconstructed signal.
  - (iv) Square the above signal and compute the FFT.
  - (v) Add up peak magnitudes of the third, fourth, and fifth peaks of the squared signal in frequency domain.
  - (vi) Repeat substeps (i)–(v) by varying the amplitude  $A_3$  systematically, until the minimum sum in (v) is achieved. The corresponding value of  $A_3$  will be the one to be pursued.
- (h) Use an approach similar to step (g) to determine the amplitudes  $A_4$  and  $A_5$  of  $4f_1$  and  $5f_1$  components, while  $V(t)$  in the second substep of (g) includes all already reconstructed frequency components.
  - (i) Reconstruct the rectified signal by taking  $V(t) = \sum_{i=1}^5 A_i \sin(2i\pi f_1 t + \phi_i)$ .
  - (j) Reset the zero level of the reconstructed signal by subtracting its minimum from it.
  - (k) Take the square and compute the FFT; then utilize Eqs. (10) and (11) to derive the amplitude  $A$  and offset  $B$  of the recovered signal, which is as defined in Eq. (1). Note that the initial phase angle  $\phi_1$  has already been obtained in step (e).

### V. EXPERIMENTAL VALIDATION

To validate this mathematical recovery process, both conventional and microfabricated HWAs were employed for real flow measurements. In the present research, a dipole field was generated to serve this purpose. From pointwise measurements under specified experimental conditions, three typical time traces were selected for case studies that further interpret the recovery method. The overall field measurement results were then compared, in the format of recovered velocity amplitude distribution, with the analytical model.

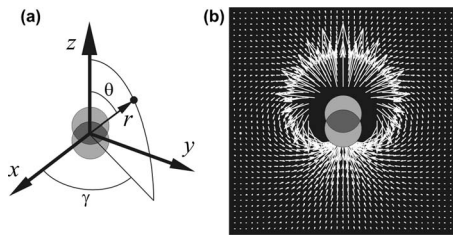


FIG. 4. Coordinates associated with a dipole source (a) and vector pattern of the velocity amplitudes in  $y$ - $z$  plane (b). The latter was generated from analytical model; the dipole vibration axis coincides with the  $z$ -axis.

### A. Analytical model, experimental setups, and HWA calibration

While a sphere vibrates in water, it generates a dipole field. This flow phenomenon has been well studied analytically based on potential flow assumption.<sup>16</sup> For a sphere vibrating sinusoidally along the  $z$ -axis with its center of vibration at the origin, as defined in Fig. 4(a), the water particles oscillate sinusoidally at the same frequency with the dipole source (the vibrating sphere). In the near field the amplitude distribution of oscillating velocity ( $U$ ) is given as

$$U = \left( \frac{a^3}{r^3} 2\pi f_1 A \cos \theta \right) \hat{i}_r + \left( \frac{a^3}{r^3} \pi f_1 A \sin \theta \right) \hat{i}_\theta, \quad (18)$$

where  $a$  is the diameter of the sphere,  $f_1$  and  $A$  are the vibration frequency and amplitude of the sphere, and others as defined in Fig. 4(a). Figure 4(b) provides an overview of the amplitude distribution of oscillating velocity in the  $y$ - $z$  plane based on this analytical model.

Experimentally, the dipole field was generated in a water tank by vibrating a sphere in certain directions using a minishaker (B&K, model 4010). Figure 5(a) shows one setup for conventional HWAs (Dantec Dynamics, model 55R11). The sensing wire of each HWA is a cylindrical quartz fiber of diameter of  $70 \mu\text{m}$  and length of 3 mm covered by a nickel

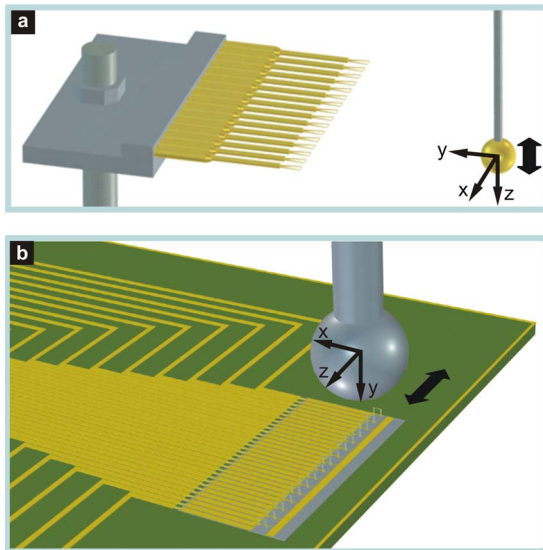


FIG. 5. (Color online) Experimental setups for dipole field measurements using conventional HWAs (a) and microfabricated HWAs (b). Black arrows indicate dipole vibration directions (along  $z$ -axis), and the flow velocity imposed on a hot wire is perpendicular to its longitudinal axis for both types of HWAs.

thin film of thickness of  $2 \mu\text{m}$ . The dipole field was created by a sphere of diameter of 12.7 mm. The sphere vibrated perpendicularly to the conventional HWA array, with 1.5 mm amplitude at 75 Hz. Figure 5(b) shows another setup for microfabricated HWAs.<sup>4</sup> The sensing wire is of length  $400 \mu\text{m}$  and is elevated  $600 \mu\text{m}$  above the surface of the substrate. The wire consists of a nickel filament that is sandwiched by two layers of polyimide; the cross section of the nickel film is  $4 \mu\text{m}$  wide by  $0.12 \mu\text{m}$  thick, and the polyimide beam is  $6 \mu\text{m}$  wide by  $2.7 \mu\text{m}$  thick. The dipole field to test the microfabricated HWAs was generated by a sphere of 6.35 mm diameter vibrating along the microfabricated HWA array, with 0.4 mm amplitude at 75 Hz. In each setup 16 HWAs were involved, but only one near the center of the array was used for measurements. Both types of HWAs were operated in constant temperature mode at an overheat ratio of 0.1. For data acquisition, a total of 4096 samples was recorded at a sampling rate of 2048 samples/s from each HWA.

It is commonly known that HWAs do not respond linearly to flow velocity in steady flows. For oscillating flows, HWA outputs can be further affected by the amplitude and frequency of the flow in a nonlinear fashion. This nonlinear behavior leads to distortion of a signal and increase in the voltage at flow reversal.<sup>25-28</sup> For oscillating flows at low amplitudes, which is the focus of the present research, the signal distortion due to the flow reversal might be insignificant.<sup>29</sup> Therefore, the HWAs employed in the experiments were calibrated in steady flows only. Specifically, the HWAs attached to a fixture were towed by a high precision linear stage (Newport model IMS600PP) in quiescent water step by step throughout the velocity range of interest. The obtained nonlinear calibration formulas, which abide by King's law, were then applied to convert voltage signals to velocity signals and to correct the signal distortion to certain extent. For complex flows with strong fluctuations, a comprehensive calibration procedure accounting for frequency and flow reversal effects is demanding.

### B. Case studies on time-trace recovery

To demonstrate how the advanced recovery method works on real-world signals, case studies are presented in the following. Three typical cases are chosen to represent commonly encountered situations, such as signals from different types of HWAs, under different levels and directions of dc shift, and with different signal-to-noise ratios. The focus is on reconstruction of an idealized form of a rectified signal only. Further recovery of such an idealized rectified signal is straightforward, as described in detail in Sec. II.

#### 1. Case 1: Oscillating flow with large dc shift

The acquired signal is from a conventional HWA, as illustrated in Fig. 5(a). The center of the HWA sensing filament was located at  $(x, y, z) = (0, 14.5 \text{ mm}, 0)$ , referring to the coordinates defined in Figs. 4(a) and 5(a). As shown in Fig. 6(a), the original time trace is converted from voltage to velocity by applying nonlinear calibration formulas. It clearly demonstrates the occurrence of rectification, but the waveform differs from a standard rectified waveform as typi-



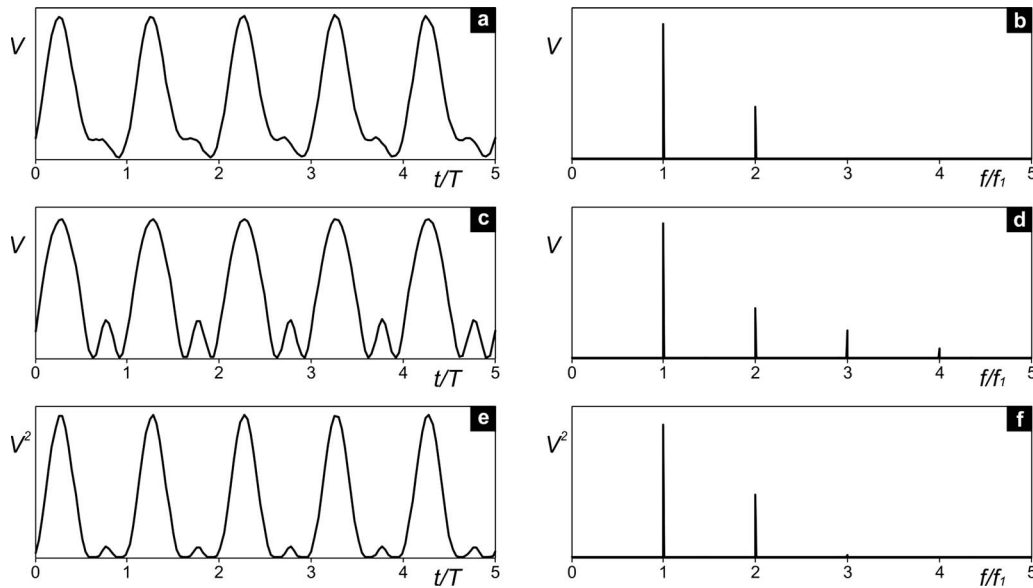


FIG. 6. Waveforms and corresponding amplitude spectra for an original signal [(a) and (b)], reconstructed signal [(c) and (d)], and squared reconstructed signal [(e) and (f)]. The original signal was acquired from a conventional HWA in a dipole field and was converted from voltage to velocity by applying nonlinear calibration formulas. The velocity amplitude of the local flow at the measurement position was 29.5 mm/s.

cally presented in Fig. 1(c). This kind of waveform distortion is mainly caused by the loss of rectification-induced higher frequency components, which is evident in Fig. 6(b). Furthermore, in this case the frequency component at the stimulus frequency  $f_1$  was still dominant over the  $2f_1$  component, meaning that a relatively strong dc flow has been superimposed to the sinusoidal oscillation of water particles, at least locally. Note that in this case the local oscillating flow to the HWA is vertical and is affected by the natural convection generated by the hot wire.

To recover the rectified signal, the procedure discussed in Sec. IV has been followed. Due to the fact that the  $2f_1$  component is weaker, to ensure a better accuracy, the  $f_1$  component was used to determine the phase information of all higher frequency components. Based on that, the corresponding amplitudes of these components were further determined, and the reconstructed rectified signal was presented in Fig. 6(c) in the time domain and Fig. 6(d) in the frequency domain. It is evident that after reconstruction, the lost higher-frequency components were regenerated reasonably [Fig. 6(d)]. The waveform was also corrected without losing the main features of its original [Fig. 6(c)]. By squaring the reconstructed signal [Fig. 6(e)], indeed all the frequency components after  $2f_1$  disappeared [Fig. 6(f)]. A further recovery from the reconstructed rectified signal using the schemes discussed in Sec. II yields a nearly perfect sinusoidal signal as expected (not shown).

## 2. Case 2: Oscillating flow with small dc shift

The signal treated was from a microfabricated HWA [Fig. 5(b)]. The HWA sensing filament was located at  $(x, y, z) = (0, 7.5 \text{ mm}, 0)$ , referring to the dipole coordinates defined in Figs. 4(a) and 5(b). In this case the sensing filament of a microfabricated HWA is much smaller than that of a conventional HWA; therefore the generated natural convection is much weaker. More importantly, the local oscillating

flow to the HWA is horizontal, and the natural convection has much less effect on it. With a resulting weak dc flow superimposed on a relatively strong oscillation of water particles, the rectification surely will diminish the  $f_1$  component of the measured signal and make the  $2f_1$  component dominant. This has been verified by experimental results, as shown in Figs. 7(a) and 7(b). To achieve a better recovery for this case, obviously the determination of phase information for all frequency components should be based on the  $2f_1$  component instead of the  $f_1$  component used in case 1. The reconstructed rectified signal is presented in Figs. 7(c) and 7(d), and the squaring method verifies a perfectly rectified signal, as is evident in Figs. 7(e) and 7(f).

## 3. Case 3: Oscillating flow with effect of background noise

In cases 1 and 2 as discussed in the foregoing, background noise is negligible due to the very high signal-to-noise ratio. In order to examine the effect of the background noise, the same experimental setup and conditions in case 2 were employed for the present case, except that the microfabricated HWA was moved further away from the dipole source to achieve a relatively low signal-to-noise ratio. Specifically, the sensor was placed at  $(x, y, z) = (0, 12.5 \text{ mm}, 0)$ , referring to the dipole coordinates defined in Fig. 4(a) and 5(b). According to Eq. (18), the velocity amplitude in a dipole field decreases at the rate of  $1/r^3$ .

The original signal and the corresponding spectrum are presented in Figs. 8(a) and 8(b). The waveform distortion due to background noise is surely severe. For recovery, however, the same procedure with case 2 was followed, and no additional efforts were needed to deal with the noise. In fact, the recovery method itself is of noise-filtering functionality since during reconstruction process, all the frequency components out of interests have been discarded, including the background noise. The reconstructed rectified signal and its

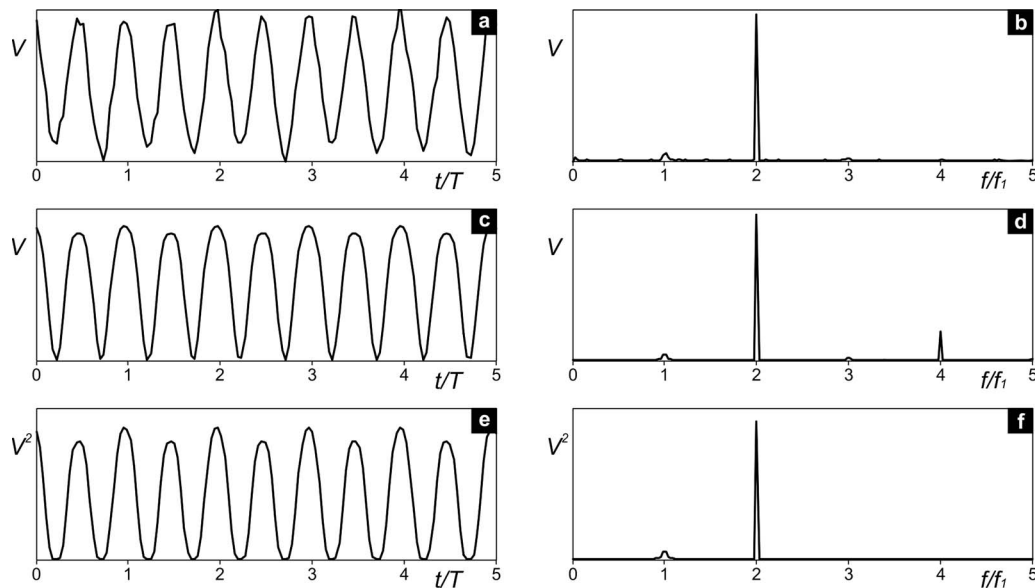


FIG. 7. Waveforms and corresponding amplitude spectra for an original signal [(a) and (b)], reconstructed signal [(c) and (d)], and squared reconstructed signal [(e) and (f)]. The original signal was acquired from a microfabricated HWA in a dipole field relatively close to the dipole source and was converted from voltage to velocity by applying nonlinear calibration formulas. The velocity amplitude of the local flow at the measurement position was 7.3 mm/s.

spectrum are shown in Figs. 8(c) and 8(d). It is evident that this new signal resembles its original but has a clear background. The signal squaring, as illustrated in Figs. 8(e) and 8(f), once again verified that this reconstructed signal was an ideal rectified waveform since no frequency components beyond the second one were observed.

### C. Amplitude comparison between recovered results and analytical model

To examine the accuracy of the recovery method and to demonstrate its general applicability, experimental results from conventional HWAs are compared with the analytical model.

For a conventional HWA, by traversing it step-by-step along the path  $y=15$  mm and  $z=0$ , the amplitude distribution of the oscillating flow velocity from the dipole field was first obtained. As presented in Fig. 9(a), the amplitude distributions for both  $f_1$  and  $2f_1$  components directly from original rectified signals biased away from the analytical prediction. However, after the recovery, the amplitude distribution at stimulus frequency  $f_1$  matched perfectly with the analytical one. Figure 9(b) shows more measurement results; they were achieved by locating the HWA to evenly distributed grids in an area as specified in the inset of Fig. 9(b). Comparing that with the analytical counterpart [Fig. 9(c)], it is

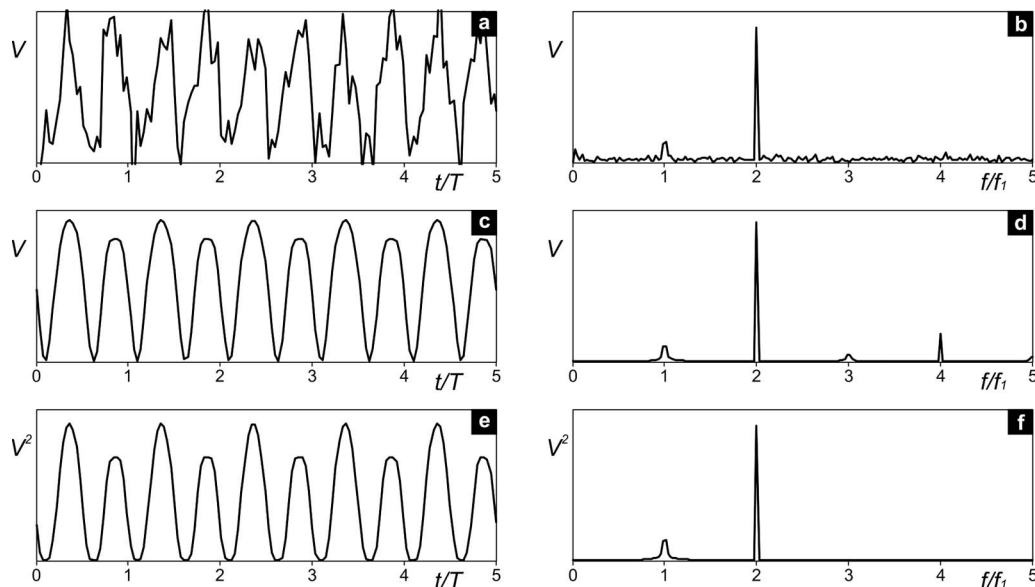


FIG. 8. Waveforms and corresponding amplitude spectra for an original signal [(a) and (b)], reconstructed signal [(c) and (d)], and squared reconstructed signal [(e) and (f)]. The original signal was acquired from a microfabricated HWA in a dipole field relatively far away to the dipole source and was converted from voltage to velocity by applying nonlinear calibration formulas. The velocity amplitude of the local flow at the measurement position was 1.5 mm/s.

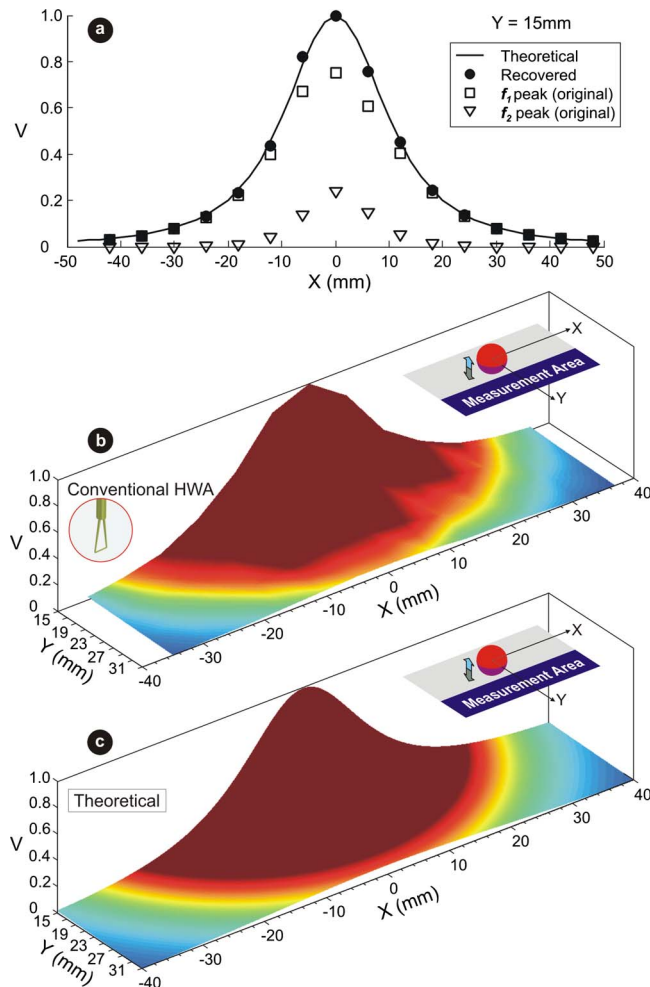


FIG. 9. (Color online) Amplitude distribution of oscillating flow velocity in a dipole field. (a) Comparison of analytical model with conventional HWA measurements before and after recovery along a specified path. (b) Recovered measurement results from conventional HWA in an area of the dipole field as specified in the inset. (c) Results from analytical model in the same area of the dipole field. In all the plots velocity amplitude was normalized by its maximum value. The maximum value was 27.3 mm/s for plots (a) and (b) and 26.8 mm/s for (c). The arrows in the insets of (b) and (c) indicate dipole vibration direction.

convincing that they matched extremely well over the entire measurement area.

## VI. CONCLUSIONS

A recovery method for rectified oscillatory hot-wire signals has been developed. The signal rectification happens when a HWA is exposed in a flow with local flow reversal. During measurements interferences are diverse and inevitable; the sources can be dc shifts as well as background noise. The loss of some rectification-introduced frequency components makes the signal even more complex. The developed method is capable of dealing with all these issues. It

is based on the reconstruction of a Fourier series expansion by applying analytically derived phase relationships among terms and by squaring the signal to determine coefficients. To ensure the best faithfulness between the reconstructed signal and its original, different cases have been studied experimentally by employing both conventional and microfabricated HWAs. The method was further applied to the measurements of a dipole field—a flow field created by a vibrating sphere in still water, and the recovered data matched very well with the analytical model.

## ACKNOWLEDGMENTS

This work was funded by Defense Advanced Research Projects Agency (DARPA) under BioSenSE program, Contract No. FA 9550-05-1-0459.

- <sup>1</sup>F. Jiang, Y. C. Tai, C. M. Ho, R. Karan, and M. Garstener, IEDM'94, San Francisco, CA, 1994 (unpublished).
- <sup>2</sup>T. Neda, K. Nakamura, and T. Takumi, *Sens. Actuators, A* **54**, 626 (1996).
- <sup>3</sup>T. Ebefors, E. Kalvesten, and G. Stemme, Proceedings of IEEE MEMS'98, Heidelberg, Germany, 1998 (unpublished).
- <sup>4</sup>J. Chen and C. Liu, *J. Microelectromech. Syst.* **12**, 979 (2003).
- <sup>5</sup>L. v. Ngo, W. Kupke, H. Seidel, and U. Schmid, CANEUS Conference on Micro-Nano-Technologies, Monterey, CA, 2004 (unpublished).
- <sup>6</sup>Y. Yang, J. Chen, J. Engel, S. Pandya, N. Chen, C. Tucker, S. Coombs, D. L. Jones, and C. Liu, *Proc. Natl. Acad. Sci. U.S.A.* **103**, 18891 (2006).
- <sup>7</sup>S. Pandya, Y. Yang, D. L. Jones, J. Engel, and C. Liu, *EURASIP J. Appl. Signal Process.* **2006**, Article ID 76593 (2006).
- <sup>8</sup>S. Coombs, R. R. Fay, and J. Janssen, *J. Acoust. Soc. Am.* **85**, 2185 (1989).
- <sup>9</sup>U. R. Müller, *Exp. Fluids* **13**, 208 (1992).
- <sup>10</sup>C. Yao, F. Chen, D. Neuhart, and J. Harris, Second AIAA Flow Control Conference, Portland, OR, 2004 (unpublished).
- <sup>11</sup>H. H. Bruun, *Hot-Wire Anemometry: Principles and Signal Analysis* (Oxford University Press, Oxford, 1995).
- <sup>12</sup>P. M. Handford and P. Bradshaw, *Exp. Fluids* **7**, 125 (1989).
- <sup>13</sup>J. H. Wamuff, A. E. Perry, and M. S. Chong, *Exp. Fluids* **1**, 63 (1983).
- <sup>14</sup>Y. Li and A. Naguib, *AIAA J.* **43**, 520 (2005).
- <sup>15</sup>T. Persoons, A. Hoefnagels, and E. d. Bulck, *Exp. Fluids* **40**, 555 (2006).
- <sup>16</sup>A. J. Kalmijin, in *Sensory Biology of Aquatic Animals*, edited by J. Atema, R. R. Fay, A. N. Popper, and W. N. Tavolga (Springer, New York, 1988), pp. 83–130.
- <sup>17</sup>E. G. Drucker and G. V. Lauder, *J. Exp. Biol.* **203**, 2379 (2000).
- <sup>18</sup>E. D. Tytell and G. V. Lauder, *J. Exp. Biol.* **207**, 1825 (2004).
- <sup>19</sup>M. H. Dickinson, F.-O. Lehmann, and S. P. Sane, *Science* **284**, 1954 (1999).
- <sup>20</sup>X. Tian, J. Iriarte-Diaz, K. Middleton, R. Galvao, E. Israeli, A. Roemer, A. Sullivan, A. Song, S. Swartz, and K. S. Breuer, *Bioinsp. Biomim.* **1**, S10 (2006).
- <sup>21</sup>M. A. MacIver, E. Fontaine, and J. W. Burdick, *IEEE J. Ocean. Eng.* **29**, 651 (2004).
- <sup>22</sup>J. Yu, M. Tan, S. Wang, and E. Chen, *IEEE Trans. Syst. Man Cybern.* **34**, 1798 (2004).
- <sup>23</sup>Y. Yang and D. Rockwell, *J. Fluid Mech.* **520**, 267 (2004).
- <sup>24</sup>S. Dong, G. E. Karniadakis, A. Ekmekci, and D. Rockwell, *J. Fluid Mech.* **569**, 185 (2006).
- <sup>25</sup>T. J. Pedley, *J. Fluid Mech.* **67**, 209 (1975).
- <sup>26</sup>T. J. Pedley, *J. Fluid Mech.* **78**, 513 (1976).
- <sup>27</sup>D. F. Elger and R. L. Adams, *J. Phys. E* **22**, 166 (1989).
- <sup>28</sup>G. Huelsz and F. Lopez-Alquicira, *Exp. Fluids* **30**, 283 (2001).
- <sup>29</sup>P. Freymuth, *J. Phys. E* **10**, 705 (1977).